Fusion Engineering and Design 219 (2025) 115276

Contents lists available at ScienceDirect

Fusion Engineering and Design

journal homepage: www.elsevier.com/locate/fusengdes

Variable-Depth Complementary Spiral cooling channel design for the steerable ECRH mirrors of DTT

Alfredo Pagliaro [a,*], Francesco Braghin [a], Alessandro Bruschi [b], Daniele Busi [a], Eliana De Marchi [c], Francesco Fanale [b], Gustavo Granucci [b,d], Afra Romano [d,e], Fabio Zanon [c]

[a] Politecnico di Milano, Department of Mechanical Engineering, Via Giuseppe La Masa 1, Milano 20156, Italy
[b] Institute for Plasma Science and Technology, National Research Council of Italy, Via Roberto Cozzi 53, Milano 20125, Italy
[c] Eni S.p.A., Piazzale Enrico Mattei 1, 00044 Roma, Italy
[d] DTT S.C. a r.l., Via E. Fermi 45, Frascati, 00044 Roma, Italy
[e] ENEA, Technology for Nuclear Safety and Security Department, Via Enrico Fermi 45, Frascati, 00044 Roma, Italy

ARTICLE INFO

Index Terms:
Heat sink
Microwave technology
Steering mirror
CFD
ECRH

ABSTRACT

The steerable launching mirrors, essential for directing microwave beams into the plasma, play a pivotal role in the Electron Cyclotron Resonance Heating (ECRH) system for the Divertor Tokamak Test (DTT) facility, currently under construction in Frascati, Italy. Due to the substantial heat and electromagnetic induced loads acting on the mirrors, implementing internal channels for active water cooling, together with a proper choice of the materials, is necessary to keep temperature and deformation under control. Three different channel configurations are studied. First, the single-channel spiral cooling path with a constant cross-section, defined in a previous design stage, has been examined. Then, a constant-depth complementary spiral geometry that increases heat exchange area has been defined and analyzed. Finally, a variable-depth complementary spiral channel is proposed and optimized to increase heat exchange efficiency. In all cases, single-channel geometries are considered to enhance safety and malfunctioning detectability. The study is based on Computational Fluid Dynamics simulations. In order to reduce electromagnetic loads on the mirrors in case of plasma disruption to a tolerable extent, a reduced electrical conductivity of the mirror bulk material with respect to pure copper is necessary: this requires the use of material different than copper alloys, which have in turn a lower thermal conductivity. In this case, high cooling efficiency is mandatory. With this goal in mind, first, the performances of the different configurations in terms of mirror temperature and pressure drop are compared considering a reference material with 100 W/(m·K) thermal conductivity. Then, the variable-depth configuration is tested for different and more realistic mirror materials. Finally, a comparison between the developed geometry and previous solutions is provided.

1. Introduction

The Divertor Tokamak Test (DTT) facility [1], under construction in Frascati, Italy, is aimed at testing different divertor configurations in DEMO-relevant conditions. The DTT project is supported by the Italian government and other contributors like Eni, CNR, and ENEA. To be relevant for future machines like DEMO, the divertors tested in DTT will be subjected to high heat fluxes. This involves the utilization of a robust Heating and Current Drive system, incorporating methods such as Neutral Beam Injection, Ion Cyclotron Resonance Heating, and Electron Cyclotron Resonance Heating (ECRH). In particular, the ECRH system will feature a total installed power of 32 MW, with 161-MW gyrotrons for the first DTT phase and already under procurement, operating at 170 GHz for a pulse duration of 100 s [2]. The 32 front-steering launchers will be distributed across 4 sectors of the machine, equipped with equatorial and upper antennas with 6 and 2 launchers each, respectively [3]. The gyrotrons are arranged in four clusters, each consisting of eight sources. The power generated by each cluster is transmitted via a quasi-optical, evacuated multibeam transmission line [4] to two launchers located at the equatorial and upper ports of the DTT. There, the beams are injected into the plasma using independently steerable mirrors [5]. During beam reflection, ohmic losses occur in the conductive materials, causing significant thermal loads on launcher mirrors' surfaces, particularly on the steering mirrors, which are further

* Corresponding author.
E-mail address: alfredo.pagliaro@polimi.it (A. Pagliaro).

https://doi.org/10.1016/j.fusengdes.2025.115276
Received 13 January 2025; Received in revised form 6 May 2025; Accepted 12 June 2025
Available online 26 June 2025
0920-3796/© 2025 The Author(s). Published by Elsevier B.V. This is an open access article under the CC BY license (http://creativecommons.org/licenses/by/4.0/).

compounded by nuclear loads from the plasma chamber. Given the relatively long duration of plasma pulses, an active water-cooling system is necessary to keep mirrors temperature and deformation under control [6]. Typically, the cooling is provided through dedicated channels dug in the mirror bulk. In the case of the launcher mirrors in EAST [7] and KSTAR [8], these channels follow an S-shaped trajectory, while in W7-X [9,10] and some launcher mirrors for ITER [11] a spiral path is adopted. Other mirrors utilize serpentine cooling configurations [12,13]. Each launcher includes one fixed focusing mirror (M1) and one planar steering mirror (M2), which will be subject to nuclear and radiative heat loads from the plasma, as well as heating due to microwave absorption.

In addition to thermal loads, high electromagnetic forces acting on the mirrors are expected during plasma disruption. An estimation of these electromagnetic effects was preliminary addressed in [14] with corresponding torques acting on the copper launching mirrors of up to 11.9 kNm. To reduce such loads, the use of different materials with lower electrical conductivity for the bulk of the mirrors is required. Since these kinds of materials are characterized also by a lower thermal conductivity, an improvement of thermal performances is needed, changing the geometry of the cooling channel. Therefore, the aim of this work is the evaluation of thermal performances for various geometric configurations of M2 internal cooling channels via computational fluid dynamics (CFD) analyses, with a focus on the development of a customized cooling channel geometry, aimed at optimizing heat transfer even for materials with low thermal conductivity, like 316 L stainless steel (SS).

The optimization of channel geometry was based on configurations of the M2 mirror analysed in previous studies. Among the analysed solutions, the single-channel spiral configuration leads to prohibitive mirror temperatures when considering SS as mirror material [15]. On the other hand, a radial configuration with multiple channels in parallel showed better thermal performances [15] but could pose a higher safety risk in the event of a difficult-to-detect channel malfunctioning, like one of the parallel branches getting blocked. Lastly, a novel geometry based on Triply Periodic Minimal Surfaces (TPMS) was considered for the steering mirror in [16]. To ensure a safe and easily machinable cooling system, the geometry hereafter presented was chosen to be in single-channel configuration, optimized to ensure acceptable temperatures even in materials with low thermal conductivity.

Three different cooling channel geometries of increasing complexity and effectiveness are analyzed:

1. a simple elliptic spiral with constant cross-section;
2. a constant-depth complementary elliptic spiral;
3. a variable-depth complementary elliptic spiral.

In all cases, no bifurcations are present in the channel. The main advantage of a single-channel configuration is its intrinsic safety, as it ensures prompt identification of any issues related to fluid flow, like pressure and flow rate fluctuations either due to leaks, cracks in mirror material or to solid particles obstructing the channel.

First, the analysis of the three geometries is performed using a reference mirror material with thermal conductivity of 100 W /(m·K) Finally, an optimized variable-depth geometry is tested for different and more realistic mirror materials, over a range of thermal conductivity values between 15 and 350 W/(m·K)

2. M2 mirror

The steerable mirrors (M2) of all DTT ECRH launchers have the same geometry to increase modularity. The M2 mirror is an elliptic plate with a minor radius of 69 mm, a major radius of 132 mm and a thickness of 10 mm, as illustrated in Fig. 1. The thickness is selected to ensure adequate structural strength. In this study, a minimum thickness of 2 mm was considered for both the frontal and rear sections, while 6 mm are occupied in-between by internal channels.

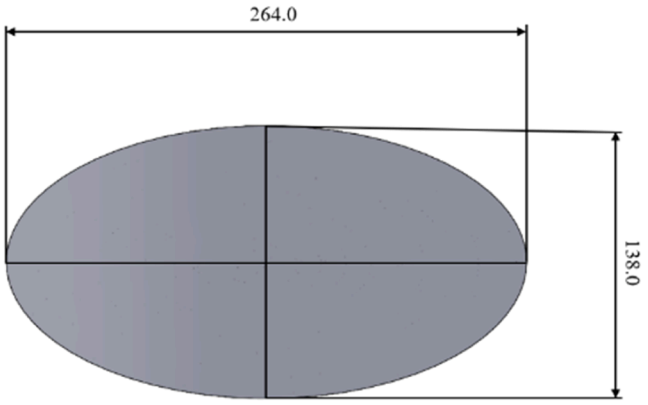

Fig. 1. Geometry of M2 mirror reflective surface.

M2 is a plasma-facing component placed inside the ECRH port. Consequently, the reflective surface is subjected to the following three heat loads [17]:

- volumetric neutron heating, originating from the d-D fusion reactions within the plasma, with approximately uniform power density of 10 kW/m^3 across the entire mirror volume;
- radiative power from the plasma, dependent on mirror orientation, with uniform surface power density of 0.1768 MW/m^2 for an inclination angle of 45° with respect to port axis;
- absorbed surface power density from the microwave beam, characterized by the Gaussian distribution (shown in Fig. 2.) produced by the 1 MW beam:

$$P_{mw} = A_{mw} P_0 e^{-2\left(\left(\frac{x}{w_x}\right)^2 + \left(\frac{y}{w_y}\right)^2\right)}$$

Where A_{mw} is the absorption coefficient of the surface at beam frequency, x and y are spatial coordinates on surface minor and major axes, respectively, and P_0 is incident power density peak, calculated as:

$$P_0 = \frac{2Q}{\pi w_x w_y}$$

where Q is total incident beam power (1 MW), while w_x and w_y define the beam radius projected along x and y directions.

The absorption coefficient A_{mw} depends on surface material properties, beam frequency and polarization. Due to tungsten sputtering from the divertor foreseen during the life of DTT, tungsten is considered as the reference surface material (for A_{mw} computation only). The beam has a frequency of 170 GHz and parallel polarization by assumption, to account for the worst-case condition. Therefore, the absorption coeffi-

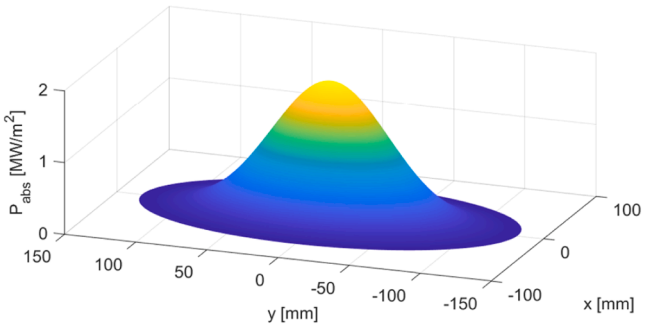

Fig. 2. Distribution of power density absorbed by mirror surface due to the incident microwave beam.

cient is computed through the following approximation [17,18]:

$$A_{mw} = \eta_r \left(\frac{4}{\cos\theta}\right) \cdot \frac{R_s}{Z_0}$$

where θ is the angle of incidence, R_s is the surface electrical resistance of tungsten at 200 °C, Z_0 is the impedance of free space, and η_r is a safety factor that accounts for the effect of surface roughness, conservatively assumed to be equal to 2 [17,18]. The values of w_x and w_y evaluated at 58° (worst case scenario) are 43 mm and 81.1 mm, respectively, leading to an absorbed power density peak $A_{mw}P_0$ of 1.874 $\left[\mathrm{MW/m^2}\right]$ To be conservative in the design of the new cooling system, the power load was considered under the worst-case scenario in each simulation.

3. Methodology

The conjugate heat transfer problem is addressed numerically under steady-state conditions utilizing the STAR-CCM+ software. The results, including velocity, pressure, and temperature fields, are examined and compared to determine the best geometric configuration for the M2 mirror. For fluid modelling in the simulations, a segregated solver is employed. Given the turbulent characteristics of the flow throughout all channel sections, the Reynolds-averaged Navier-Stokes two-layer realizable $k-\varepsilon$ turbulence model with $y+$ wall treatment is implemented. This choice of the two-layer treatment effectively manages the complexity of the fluid flow by automatically adjusting between low and high $y+$ treatments [15]. The model is well-suited for analyzing flows with rotation, separation, and significant pressure and velocity gradients, and it accurately represents the turbulence profile near the wall. Therefore, it is necessary to study the boundary layer and fluid dynamic parameters for the fluid model, such as [19,20]:

- Inlet turbulence intensity, defined as the ratio between the root-mean-square of the turbulent velocity fluctuations and the average velocity. For a fully developed pipe flow, it can be estimated from the Reynolds number as:

  $I = 0.16\ Re^{-\frac{1}{8}}$

- Turbulence length, associated with the size of eddies in the turbulent flow. For a fully developed pipe flow, the inlet turbulence length l can be estimated from the hydraulic diameter d as:

  $l = 0.07\ d$

The simulated boundary conditions are based on the operating conditions of the facility. For the inlet boundary condition, a uniform flow rate of 10 l/min and a constant temperature of 50 °C are specified, while maintaining an outlet pressure of 4 bar. Since the refrigerant fluid is water, its proprieties are defined in the fluid model according to the IAPWS-97 database [20]. This choice enables the monitoring of saturation temperature and pressure fields to check the boiling condition. Additionally, the thermal conductivity of the solid domain is defined in the solid model. For all the analyzed geometries, an elongated straight outlet portion is added, to avoid reverse flow phenomena in the simulation.

4. Spiral configuration

The starting point of this discussion is the spiral channel [15,17]. This geometry is characterized by a spiral path with constant semi-circular section with 3.5 mm radius. The dimensions illustrated in Fig. 3 show an overall thickness of 10 mm, allowing at least 2 mm both at the front from the internal cooling channel and at the rear. Accordingly, an

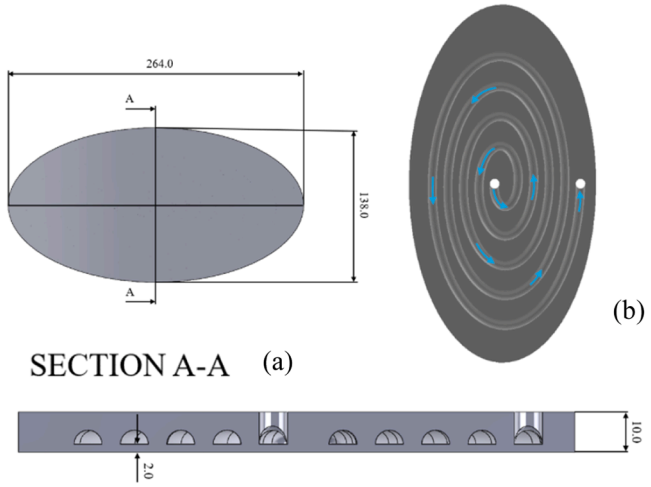

Fig. 3. Spiral cooling geometry with section view of the channels (a). The direction of the fluid flow is shown in (b).

inlet and outlet diameter of 7 mm is adopted. The mesh for the fluid and solid domains were generated to accurately describe the geometry, consistently with the turbulence model defined above.

As depicted in Fig. 4, specific parameters are crucial to achieve a fine and precise mesh that adequately captures turbulent motion. These parameters include [19,20]:

- Thickness of the boundary layer, representing the region near the wall where the fluid transition occurs.
- Number of layers required to discretize the transition region in the boundary layer.
- Thickness of the first prism layer, set according to the $y+$ parameter involved in the turbulence model.

The mesh for the simulations comprises $\sim 3.32 \times 10^6$ cells for the liquid and $\sim 4.13 \times 10^5$ cells for the solid domain.

Applying the aforementioned thermal loads results in the temperature profiles shown in Fig. 5. Due to the lower thermal conductivity of the reference material with respect to the Copper-Chromium-Zirconium (CuCrZr) case studied in [15] and [17], the temperature on the front side is relatively high. Furthermore, due to the asymmetry of channel geometry, a hotspot is observed in the upper part of the surface. The temperature field, in fact, is neither uniform nor symmetrical. Although the fluid domain exhibits a maximum temperature of 147 °C, the boiling condition is avoided. Indeed, since the local temperature at each point of the fluid domain is at least 22 °C lower than the saturation temperature at the local fluid pressure, the liquid state is preserved in all points. The computed velocity field in the spiral configuration distinctly illustrates the influence of curvature, as shown in Fig. 6. Fluid velocity tends to be

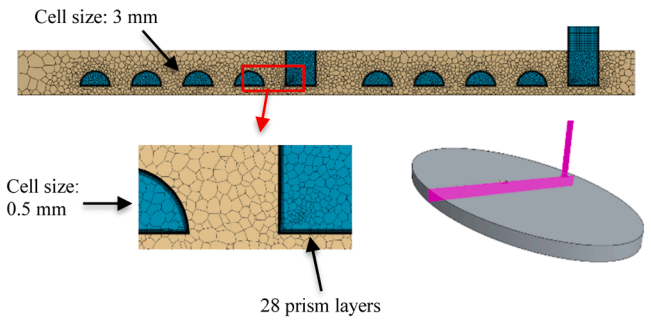

Fig. 4. Mesh configuration for CFD simulation with section view perpendicular to mirror minor axis. Spiral configuration.

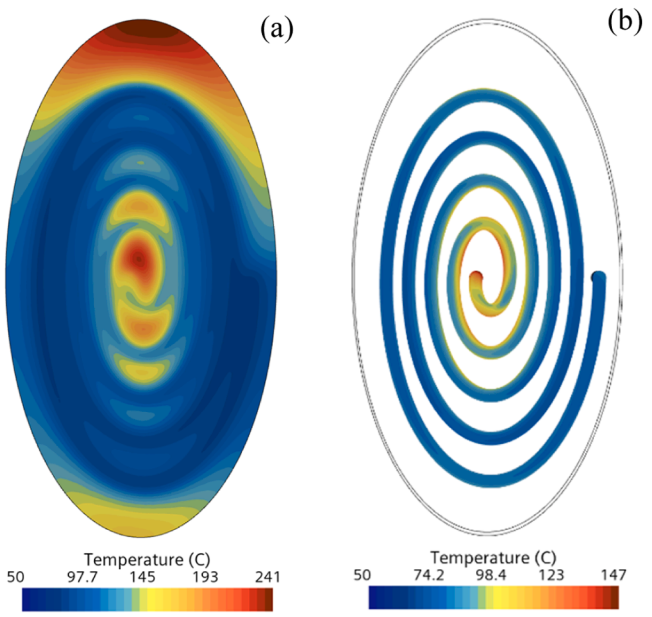

Fig. 5. Mirror (a) and fluid (b) temperature profile. Spiral cooling channel configuration.

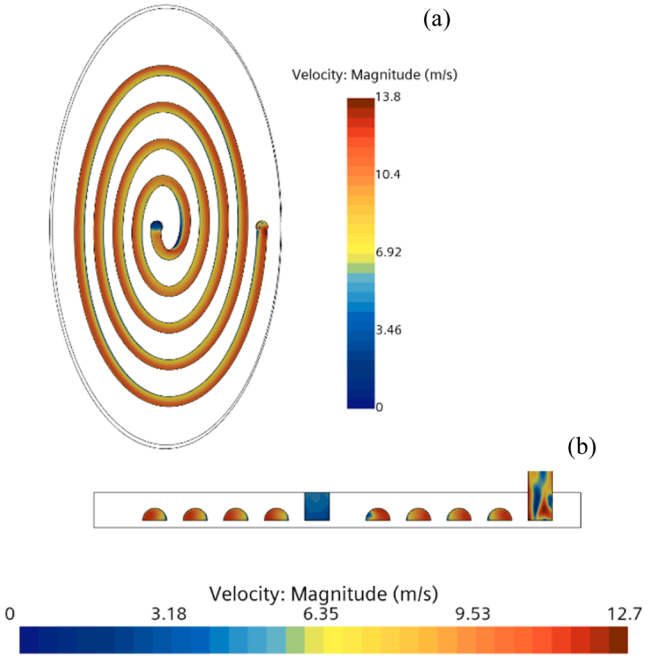

Fig. 6. (a) Fluid velocity profile in front view. (b) Fluid velocity profile in the cross-section perpendicular to the mirror minor axis. Spiral cooling channel configuration.

greater towards the outer part of each channel section. Accordingly, higher fluid temperatures are observed in the inner side of each channel section, where fluid velocity is lower. The overall pressure drop in the cooling system is 3.96 bar, with an inlet pressure of 7.96 bar, which is well below the design threshold of 11.5 bar. Due to the high temperature values and the low uniformity obtained by considering the spiral channel configuration on a material with lower thermal conductivity than CuCrZr, an optimization of this geometry is deemed necessary.

5. Constant-depth complementary spiral (CDCS) configuration

A new design of the single-channel geometry is essential to achieve a more uniform temperature profile and a lower peak value on mirror surface. Considering the potential choice of a mirror material with reduced electrical conductivity but lower thermal conductivity [14], the main target must be to maximize the exchange area between fluid and solid. This goal can be achieved by considering the complementary part of the spiral path as the fluid domain, as shown in Fig. 7.

The channel wall is created by defining its parametric equations along x and y, as follows:

$$\begin{cases} x(t) = x_0\left(\left(\frac{\vartheta}{2\pi\cdot n}\right)^{\gamma}\cos\vartheta + \delta_x\right) \\ y(t) = y_0\left(\left(\frac{\vartheta}{2\pi\cdot n}\right)^{\eta}\sin\vartheta + \delta_y\right) \end{cases}$$

with $\vartheta \in [\vartheta_0,\ 2\pi n]$.

In Table 1, the values considered for the parametric equation of the spiral are shown. As depicted in Fig. 7(a), the distance between mirror front surface and cooling channel is 2 mm, while the cooling channel domain is 2.5 mm thick, and the back plate is 5.5 mm thick. The spiral wall thickness is constant and equal to 2 mm. This implies a variable-width rectangular fluid cross-section with an inlet and outlet diameter of 5.5 mm.

The simulation has been set up with a meshing, shown in Fig. 8, results in $\sim 9.47 \times 10^6$ cells for the liquid and $\sim 8.04 \times 10^5$ cells for the solid domain.

The same boundary conditions and heat loads defined above are applied. As shown in Fig. 9, this configuration is able to improve temperature uniformity and peak value on the mirror surface, mainly due to the much larger and evenly distributed heat exchange area.

By monitoring the difference between the saturation temperature and the fluid temperature at each point in the fluid domain, we can assess that boiling is avoided. Specifically, the local temperature at each point of the fluid domain is at least 57 °C lower than the saturation temperature at the local fluid pressure.

The main drawback of the CDCS configuration is the high pressure drop of 12.9 bar, with an inlet pressure of 16.9 bar, much higher than the admissible design value of 11.5 bar. Another downside is the presence of large stagnation zones in the fluid domain, as shown in Fig. 10. Such zones correspond to hotspots in surface temperature distribution, highlighting an inefficient use of the heat exchange area.

Due to cooling channel asymmetry, a lateral hotspot is present on the surface, but with much lower temperature value (96.3 °C) with respect to the spiral configuration (241 °C).

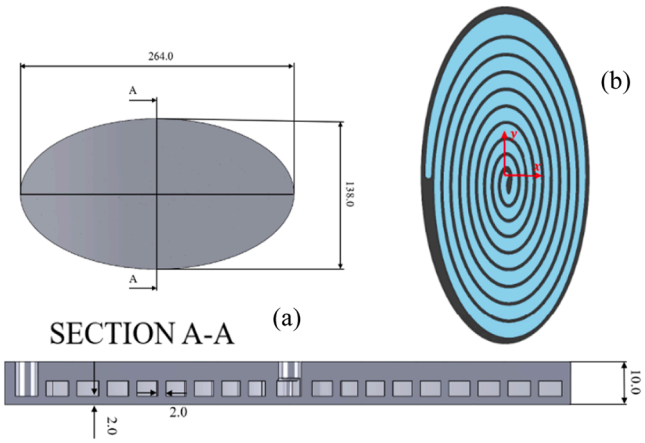

Fig. 7. (a) Section of M2 with CDCS cooling option, showing the geometry of CDCS cooling channels. (b) View of the complementary spiral channel path on the x-y plane.

Table 1
Numerical values for the complementary spiral equation parameters.

x_0 [mm]	68.5
y_0 [mm]	131.04
γ [−]	1.16
η [−]	1.12
n [−]	10.344
δ_x [−]	0.0285
δ_y [-]	-0.05

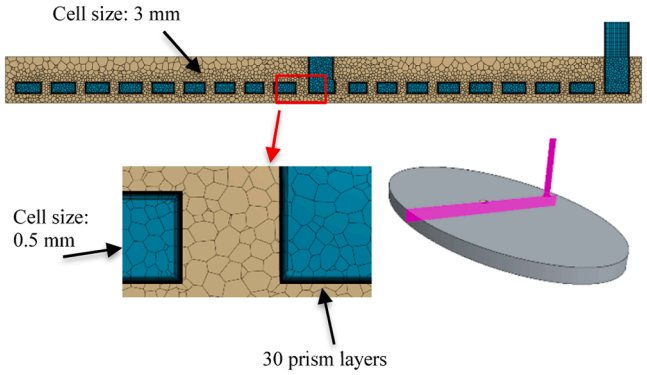

Fig. 8. Mesh configuration for CFD simulation with section view perpendicular to mirror minor axis. CDCS configuration.

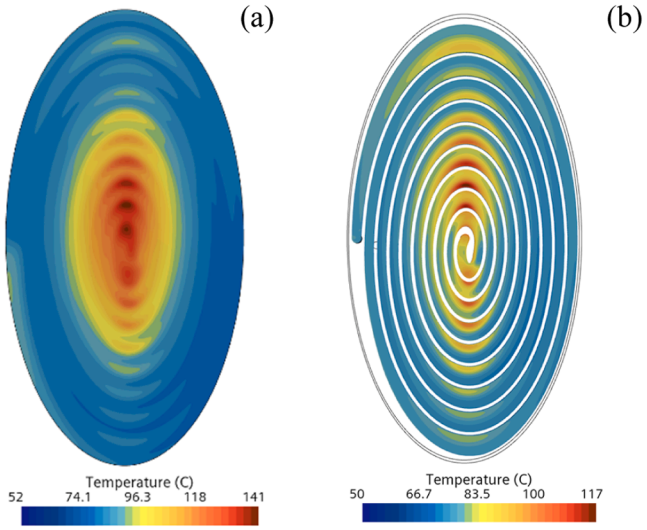

Fig. 9. Mirror (a) and fluid (b) temperature profile. CDCS configuration.

The high pressure drop and the presence of large stagnation regions suggest that there is space for further optimization, towards a more efficient use of heat exchange area. This can be achieved by a space-dependent variation of channel depth.

6. Variable-depth complementary spiral (VDCS) configuration

Starting from the CDCS design for the geometry of the M2 mirror cooling channel, a variable-depth version was developed with the aim of enhancing temperature uniformity on the mirror's surface and decreasing the pressure drop.

The constant-depth and variable-depth profiles are identical if projected on the x-y plane, the only difference being their depth (in z direction) as a function of x and y. Channel depth function $h(x, y)$, represented in Fig. 11, is given by:

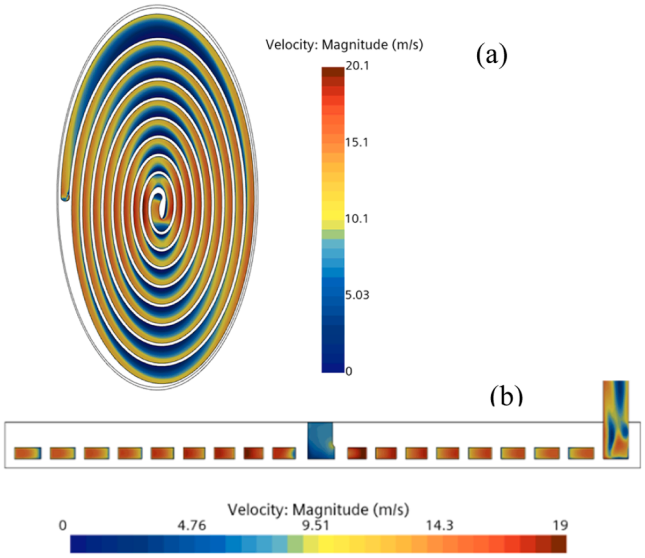

Fig. 10. (a) Fluid velocity profile in front view. (b) Fluid velocity profile in the cross-section perpendicular to the mirror minor axis. CDCS configuration.

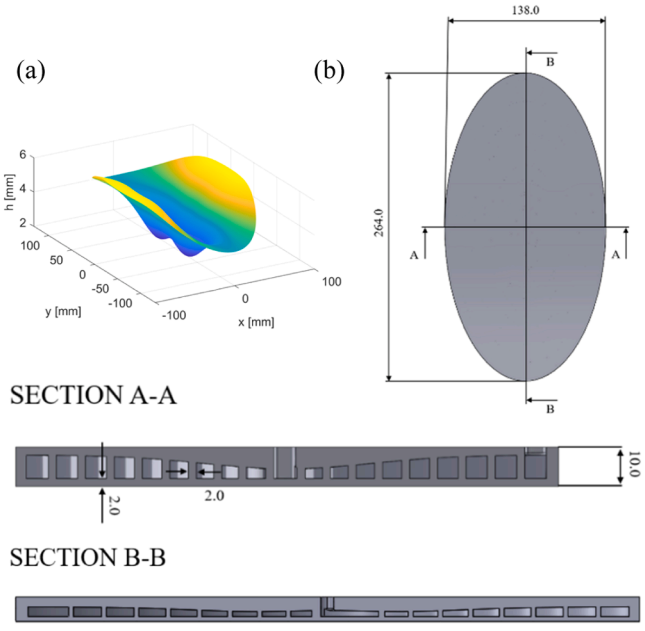

Fig. 11. Description of VDCS geometry. (a) Depth function. (b) Mirror size and section views of the channels with gaussian-sinusoidal depth profile.

$$h(x,y) = h_G(x,y) - \Delta h_S(x,y) k_S(x,y)$$

where $h_G(x,y)$ is a Gaussian contribution that follows the power density distribution of the absorbed microwave power, $\Delta h_S(x,y)$ is a sinusoidal contribution that decreases channel depth in proximity of the y axis, where channel width increases, to avoid stagnation zones, and $k_S(x,y)$ is a position-dependent coefficient to be applied to $\Delta h_S(x,y)$ so that its contribution vanishes in the origin, to avoid a singularity.

The Gaussian contribution is aimed at increasing flow velocity in the central region, where the heat flux is higher, and decreasing it in the periphery, where the heat flux is lower, to reduce the pressure drop without losing heat exchange efficiency where it's needed. The expression of the Gaussian term is:

$$h_G(x,y) = h_e - (h_e - h_0)e^{-2\left(\left(\frac{x}{w_x}\right)^2 + \left(\frac{y}{w_y}\right)^2\right)}$$

where h_e is maximum channel depth in the periphery, h_0 is minimum channel depth in the center, while w_x and w_y are equal to the radii of the elliptical trace of the microwave beam on the mirror, respectively 43 mm and 81.1 mm.

The sinusoidal contribution aims at reducing channel depth in the proximity of the y axis, where water flow slows down due to the larger channel width. The target of this contribution is to avoid stagnation zones and the corresponding hotspots along the y axis to increase temperature uniformity. The sinusoidal contribution is given by:

$$\Delta h_S(x,y) = \Delta h_0 \sin^{n_s}(\vartheta(x,y))$$

$$\vartheta(x,y) = \operatorname{atan}\left(\frac{y}{x}\right)$$

where Δh_0 is channel depth reduction in correspondence of the y axis, and n_s is related to the width of the region around the y axis that is affected by depth reduction.

The sinusoidal function is not differentiable in the origin. Therefore, a Gaussian coefficient $k_S(x,y)$ is added to asymptotically eliminate the influence of the sinusoidal term when approaching the center. We have:

$$k_S(x,y) = 1 - e^{-\kappa_s\left(\left(\frac{x}{a}\right)^2 + \left(\frac{y}{b}\right)^2\right)}$$

where κ_s determines the sharpness of the Gaussian coefficient distribution and was fixed to 20, while a and b determine its ellipticity and are equal to mirror radii, respectively 69 mm and 132 mm.

The surface associated with the depth function is generated using MATLAB (shown in Fig. 11.) and subsequently included in the CAD model through SOLIDWORKS, where channel geometry is created. The front and back plates are 2 mm thick to ensure structural integrity, and the diameter of inlet and outlet is set to 5.5 mm based on operating conditions.

Various parameters combinations in the space $(h_e, h_0, \Delta h_0, n_s)$ were tested in steady-state thermo-hydraulic simulations via STAR-CCM+ to optimize the h function. Throughout these tests, inlet water pressure and maximum water temperature were monitored. Table 2 reports a summary of the results. The combination with the lowest inlet pressure was selected:

$$h_e = 6 \text{ mm } h_0 = 2.5 \text{ mm } \Delta h_0 = 2 \text{ mm } n_s = 6$$

This combination leads to a reduction in pressure drop by 2.7 times with respect to the CDCS configuration, while preserving low mirror and water maximum temperatures, respectively 136.59 °C and 99.07 °C. Although the n_s parameter has little influence on the thermo-fluid dynamic results, a high value was preferred to ensure optimal performance, particularly in terms of pressure drop.

The simulation setup for the VDCS version of M2 follows the same guidelines as in the previous cases, and meshing was performed adapting the thickness of the boundary layer and the number of prism layers to adequately capture the fluid near the wall [19,20]. The main parameters of the mesh are illustrated in Fig. 12, resulting in $\sim 11.35 \times 10^6$ cells for the liquid and $\sim 8.66 \times 10^5$ cells for the solid domain. As anticipated earlier, the VDCS configuration successfully achieves the objective of smoothing surface temperature distribution while decreasing pressure drops. As shown in Fig. 13, the temperature on the surface is more uniform compared to the previous cases.

The pressure remains well below the design limit, with an inlet value of 8.86 bar and an overall drop of 4.86 bar. Mirror surface displays a single temperature peak of 136.59 °C at the center, where the microwave Gaussian power density reaches its highest value, as shown in Fig. 13. Simultaneously, maximum water temperature is limited to 99.07 °C. Again, since the local temperature at each point of the fluid domain is at least 57 °C lower than the saturation temperature at the local fluid pressure, the boiling condition is avoided, with larger margin compared to previous cases.

A lateral hotspot persists on mirror surface due to asymmetry of the cooling channel. This issue could be addressed by elongating the spiral by $\sim 45°$, thereby making mirror surface more symmetrical. However, since the hotspot temperature does not reach values of concern, the option of reducing hydraulic torques by aligning the inlet and the outlet on the minor axis is preferable.

The fluid velocity profile in Fig. 14 shows that the VDCS channel accelerates the fluid in the central part to enhance heat dissipation and decelerates it in the periphery to mitigate the pressure drop. Additionally, the sinusoidal pattern effectively avoids stagnation zones along the y axis and the corresponding hotspots on mirror surface.

7. Thermal performances of different mirror materials with VDCS channel

A thermal analysis was conducted considering various materials with different thermal conductivity in a range between 15 and 350 W/(m·K) The results depicted in Fig. 15 illustrate the inverse proportionality between thermal conductivity and maximum mirror and water temperatures.

For highly conductive metals and some highly conductive technical ceramics like Silicon Carbide and Aluminum Nitride

(to be used with conductive coating), temperatures remain below 150 °C. For poorly conductive metals and ceramics like Alumina, surface mirror temperatures increase, reaching 382.29 °C for SS or even 427.55 °C in the worst case (INCONEL 718). Notably, water temperature remains below 150 °C and boiling does not occur even for the lowest conducting materials.

The performance of a poorly conducting mirror can be improved by

Table 2
Steady-state thermo-hydraulic analysis results for M2 with VDCS configuration and for various $h(x,y)$ parameter combinations.

Parameters h_e, h_0, Δh_0, n_s [mm, mm, mm, -]	T_{max} [°C]		P_{inlet} [bar]
	Mirror	Water	
4, 2, 1, 1	132.5	95.0	13.5
5, 2, 1, 1	129.5	101.1	11.0
6, 2, 1, 1	131.8	107.6	9.4
4, 2.5, 1, 1	134.5	99.0	11.6
5, 2, 1.5, 1	131.9	94.3	11.8
6, 2, 1.5, 1	132.0	100.9	10.1
6, 2, 1.6, 1	132.0	99.0	10.3
4, 3, 2, 1	137.0	100.6	13.0
6, 2, 2, 1	128.1	91.8	17.2
6, 2.5, 2, 1	135.5	98.7	9.0
6, 2.5, 2, 6	136.59	99.07	8.86

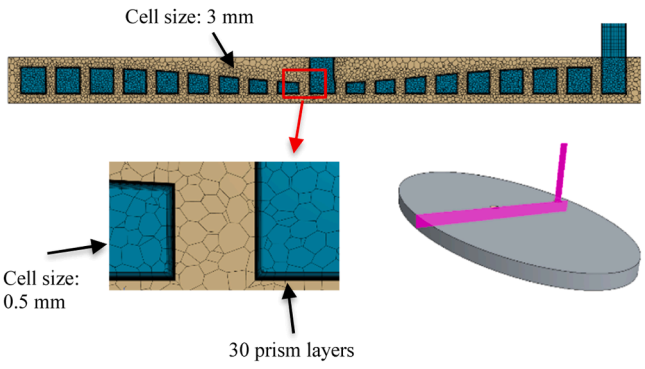

Fig. 12. Mesh configuration for CFD simulation with section view perpendicular to mirror minor axis. VDCS configuration.

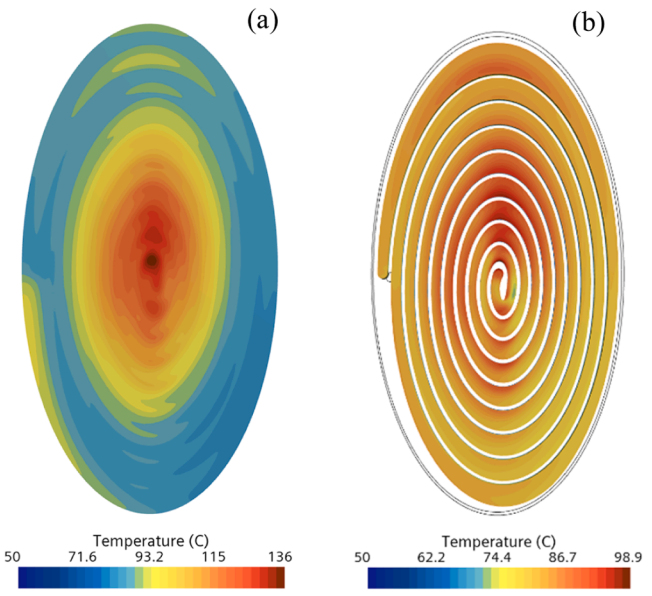

Fig. 13. Mirror (a) and fluid (b) temperature profile. VDCS configuration.

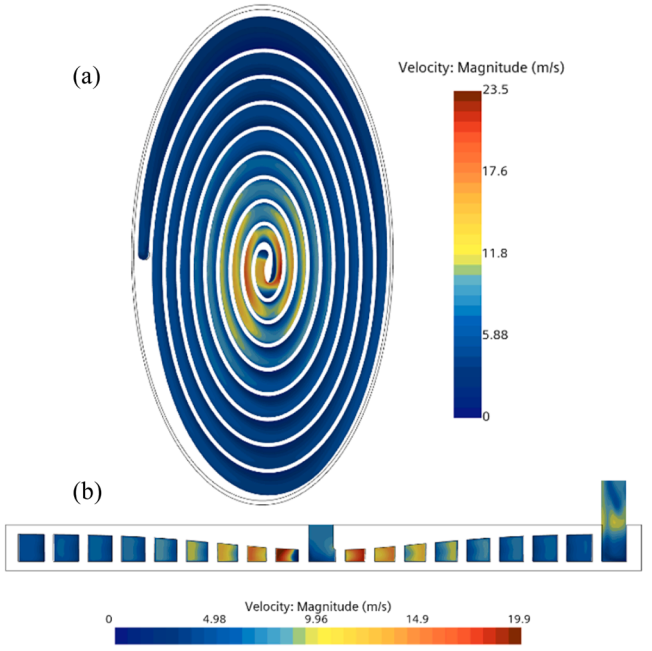

Fig. 14. (a) Fluid velocity profile in front view. (b) Fluid velocity profile in the cross-section perpendicular to the mirror minor axis. VDCS configuration.

reducing the thickness of the front surface from 2 mm to 1 mm. A test simulation was conducted on SS, resulting in the surface temperature distribution shown in Fig. 16(a). The peak temperature is still as high as 338 °C.

However, this is not due to a fundamental property of the VDCS geometry, rather it is caused by the specific shape of the inlet wall, which has larger thickness than in the rest of the spiral, as shown in Fig. 16(c). The hotspots arising in correspondence of these thicker wall portions could be easily avoided by reducing wall thickness so that it is always equal to 2 mm. To estimate the effect of such countermeasure, we consider a "probe" spot near the center, in correspondence of a 2 mm wall portion. At the probe point, the surface temperature is about 280 °C, which is about 60 °C less than at the hotspot. This shows that a slight adjustment of the VDCS inlet wall geometry could dramatically lower

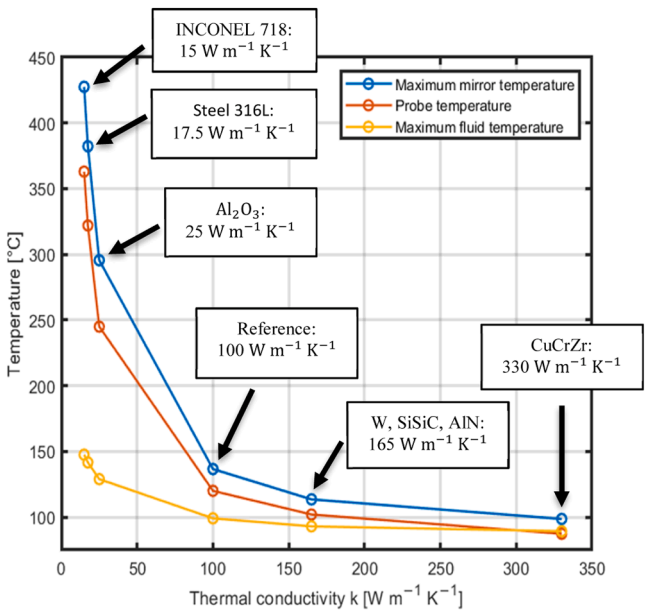

Fig. 15. Maximum mirror temperature, probe temperature (probe position shown in Fig. 16), and water temperatures as a function of the thermal conductivity of the mirror material.

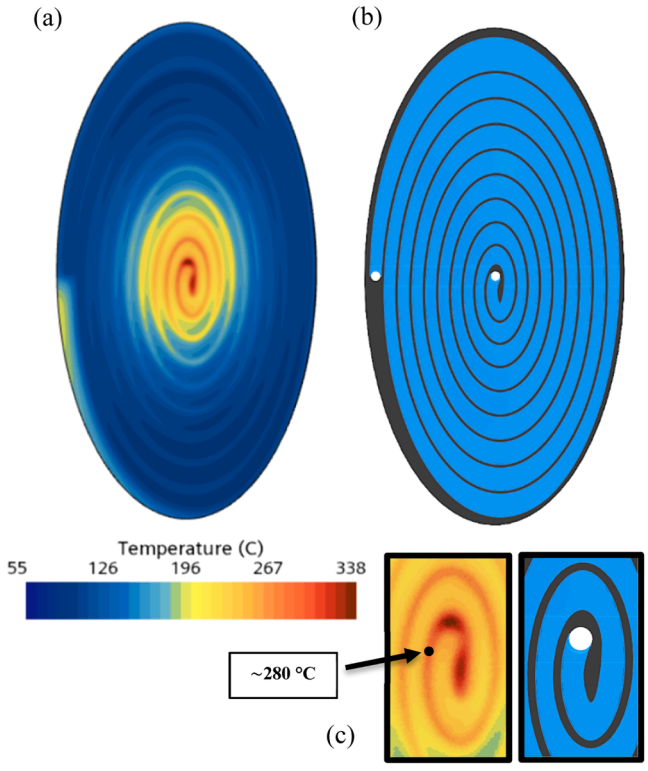

Fig. 16. Simulation of the VDCS configuration on a SS mirror with a front thickness of 1 mm. (a) Mirror temperature profile. (b) Complementary spiral channel path on the x-y plane (from Fig. 7). (c) Detailed view of the central hotspots, inlet wall shape and probe spot.

peak temperatures, and that the hotspot temperature produced by the current configuration should not be considered as representative of the potential VDCS performance, especially for poorly conductive materials.

In Table 3, the working conditions and performances of the VDCS geometry (D) are compared with those of the configurations analysed in

Table 3
Working conditions and thermohydraulic performances comparison between the VDCS geometry (D) and the other configurations: constant-section elliptical spiral (A), radial configuration (B) and TPMS (C). If two materials are specified, the first is the bulk material and the second is the front plate material. If no brackets are specified in the Material column, then the front plate is 2 mm thick, otherwise the brackets specify its thickness. If [b] is specified in the T_w column, then water boils in the channels.

ID	Geom.	Material	Working conditions				Performances		
			T_{inlet} [°C]	Q_w [l/min]	P_{abs} [MW/m^2]	ΔP [bar]	T_w [°C]	T_m [°C]	Ref.
(A1)	Spiral	CuCrZr + Cu	50	4	2.307	0.55	N.A.	152.8	[15]
(A2)		CuCrZr + Cu	50	10	2.051	2	121.3	138.1	[17]
(A3)		SS + Cu	50	4	2.307	0.55	N.A.	277	[15]
(B1)	Radial massive	CuCrZr + Cu	50	2	2.307	≈0.22	N.A.	≈180	[15]
(B2)		CuCrZr + Cu	50	4	2.307	≈0.86	N.A.	≈133	[15]
(B3)		CuCrZr + Cu	50	6	2.307	≈1.90	N.A.	≈115	[15]
(B4)	Radial lightened	SS + Cu	50	4	2.307	≈0.85	N.A [b].	330	[21]
(B5)		SS + Cu	50	4	2.307	≈0.85	N.A [b].	372	[21]
(B5)		SS	55	10	2.307	5	203 [b]	564	[16]
(C1)	TPMS	SS (1 mm)	55	10	2.307	2.8	145	243	[16]
(D1)	VDCS	Ref. 100 W/mK	50	10	2.051	4.86	99.1	136.6	This work
(D2)		CuCrZr	50	10	2.051	4.86	89.3	98.6	
(D3)		SS	50	10	2.051	4.86	141.7	382.3	
(D4)		SS (1 mm)	55	10	2.307	4.86	154.3	338.1	

previous studies: the spiral cooling channel (A), the radial geometry with multiple outlets (B) and the Triply Periodic Minimal Surface (TPMS) configuration (C). Although different mirror materials are compared, a tungsten surface coating is considered for all cases, resulting in approximately the same absorption coefficient. For the radial configuration, the massive option was considered when available, as it gives lower mirror and water temperatures than the lightened geometry [15]. For each record, we report channel geometry, mirror material, inlet water temperature (T_{in}), water flow rate (Q_w), total absorbed power (P_{abs}), inlet-outlet pressure drop (ΔP), maximum water temperature (T_w), and maximum mirror temperature (T_m). In the following, we compare the VDCS with alternative geometries.

- VDCS –spiral comparison. Considering cases (A2 - spiral) and (D2 - VDCS), we see that for the same bulk material and water flow rate, the VDCS decreases maximum mirror temperature from 138.1 °C to ≈ 100 °C, even if the absorbed power of case (D2) is 19.8 % higher and the front surface is less thermally conductive (CuCrZr vs pure Cu). This is achieved by extending the heat exchange area and increasing flow velocity where the heat flux density is maximum. The price for this increase in thermodynamic performances is an increased pressure drop, which yet remains within the acceptable range (< 7.5 bar).
- VDCS –radial comparison. Comparing cases (B4 - radial) and (D3 - VDCS) we notice that the VDCS geometry produces a much higher mirror temperature than the radial massive configuration in case of a SS mirror. However, this is due to the very different thermal conductivity of the 2 mm front layer considered in the two cases (pure Cu and SS, respectively). To make a more significant comparison between VDCS and radial configuration, we can consider the CuCrZr mirror cases (D2) and (B1, B2, B3). Thermal performances of radial channels are given for water flow rates between 2 and 6 l/min. Extrapolating the maximum mirror temperature with a hyperbolic interpolant function of the type Ax^{-a} and the pressure drop with a power law of the type Bx^b, we can roughly estimate thermal performances of the radial channel for a water flow rate of 10 l/min. The result is a maximum mirror temperature of 92 °C and a pressure drop of 5.2 bar. Both values are close to the 100 °C / 4.86 bar we get with a VDCS channel. While this is not intended to be an accurate comparison, it still supports the thesis that the VDCS channel is more convenient than a radial configuration, as it provides similar cooling effectiveness while increasing safety and manufacturing feasibility.
- VDCS –TPMS comparison. As mentioned above, a simulation with a reduced front layer thickness of 1 mm was performed, which is also the value considered by [16]. To increase comparability with the TPMS case, the same material, thermal load and boundary conditions were used. From cases (C1 –TPMS) and (D4 –VDCS), we see that the TPMS produces a much lower maximum mirror temperature than the VDCS if we include the central hotspot region. However, the difference between the "probe" temperature and the TPMS maximum temperature is about 40 °C, or 15 % (on a °C scale).

The comparisons show that the VDCS offers similar or better performances with respect to the radial and spiral configurations, even for poor thermal conductors. With proper adjustments to the details of the inlet wall structure or to the channel depth function, the developed VDCS could potentially approach the performances of much more complex structures, like the TPMS. We should stress that the upper bound to thermal performances is water speed, which could potentially cause erosion of the inner walls. The problem of quantifying erosion damage due to high water speed will be tackled in future studies.

8. Conclusions

Three distinct cooling channel geometries were examined for the DTT ECRH launcher steerable mirrors. Several CFD analyses were performed to assess thermodynamic performances of the different configurations in terms of mirror temperature distribution and fluid pressure drop. Unlike previous studies [15,16], this work focused on single-channel geometries, to privilege detectability of possible irregularities in fluid flow, either due to cracks in mirror material or to solid particles obstructing the channel. The geometries were developed considering a generic reference mirror material with a moderate thermal conductivity of 100

W/(m·K) and water as cooling fluid. The elliptic spiral option, already considered in previous studies [15,17] was taken as the starting point of the development, resulting in high mirror and water temperatures, with a peak mirror temperature of 241 °C.

A constant-depth complementary spiral (CDCS) configuration was considered as the first advancement over the spiral option, with the main target of increasing heat exchange area between solid and fluid. Although substantial improvement in mirror temperature distribution and peak value (147 °C) was achieved, this came at the cost of an unsuitably high pressure drop of 12.9 bar. Moreover, stagnant regions were found in the fluid domain, with associated hotspots on mirror surface.

These results motivated the development of a variable-depth complementary spiral (VDCS) configuration, with the aim of increasing heat exchange efficiency, reducing the pressure drop to acceptable levels and

avoiding stagnation regions.

Such solution was proved effective, with maximum mirror and water temperatures of 136.59 °C and 99.07 °C respectively, and a pressure drop of 4.86 bar. Stagnation regions in the fluid domain and the corresponding hotspots on mirror surface were also eliminated.

After developing the VDCS geometry, its performances were computed for different mirror materials. With highly conductive alloys, including technical ceramics like SiSiC and AlN, the maximum mirror temperature remains below 150 °C, with a minimum of 100 °C for the CuCrZr case. With poor conductors like Al_2O_3, SS and INCONEL 718, mirror temperature reaches values near or above 300 °C. Despite the high surface temperatures, boiling is avoided in all studied cases, as local water temperature remains below local saturation temperature in the whole fluid domain. The thermal performance of the poorly conductive mirrors can be improved by reducing the thickness of the front plate from 2 mm to 1 mm. In this way, a VDCS SS mirror shows a maximum temperature of 338.06 °C, with water maximum temperature equal to 154.31 °C. This simulation highlights the problem of a hotspot in the central region due to the details of inlet wall geometry, which could be avoided by slightly changing the shape of inlet wall portion, so that its thickness is kept constant at 2 mm. A lower maximum mirror temperature of about 280 °C is expected in this case.

The VDCS was compared with previously developed geometries, namely the elliptical spiral, the radial channels and the Triply Periodic Minimal Surfaces (TPMS) configuration. It was possible to show that the VDCS is superior in terms of thermohydraulic performances with respect to the spiral geometry, while it shows similar performances if compared with the radial geometry. The VDCS has the potential of closely approaching the performance of the TPMS geometry, when considering the improvement to mirror inlet wall shape mentioned above.

The VDCS geometry was proved to deliver good thermohydraulic performances even in the case of poorly conductive materials. Moreover, it has the advantage of increasing safety due to its single-channel configuration.

Finally, future studies will investigate the thermo-mechanical stresses experienced by the mirror launcher under both nominal heat loads and considering non-idealities in the incident power profile. Furthermore, considering that high water speed in targeted regions is key to improving thermal performance, limitations to water speed imposed by erosion damage and the effects of surface roughness on both thermal performance and pressure drop will also be assessed.

CRediT authorship contribution statement

Alfredo Pagliaro: Writing – original draft, Software, Methodology, Conceptualization. **Francesco Braghin:** Supervision. **Alessandro Bruschi:** Supervision. **Daniele Busi:** Supervision. **Eliana De Marchi:** Supervision. **Francesco Fanale:** Supervision. **Gustavo Granucci:** Supervision. **Afra Romano:** Supervision. **Fabio Zanon:** Supervision.

Declaration of competing interest

The authors declare the following financial interests/personal relationships which may be considered as potential competing interests: Daniele Busi reports financial support was provided by Eni SpA. Francesco Braghin reports financial support was provided by Eni SpA. Alfredo Pagliaro has patent pending to CNR, ENI, POLITECNICO of MILANO. If there are other authors, they declare that they have no known competing financial interests or personal relationships that could have appeared to influence the work reported in this paper.

Acknowledgements

The work was carried out as part of the DTT activities, in the context of Eni-CNR JRA. The authors wish to thank all colleagues involved in the project for their precious contributions to its completion. The paper deals with the filed patent application for a “device and use of the device for reflecting microwave radiation during electron-cyclotron resonance heating”.

Data availability

The data that has been used is confidential.

References

[1] F. Romanelli, et al., Divertor Tokamak Test facility project: status of design and implementation, Nucl. Fus. 64 (Sept 2024), https://doi.org/10.1088/1741-4326/ad5740.
[2] S. Garavaglia, et al., Progress of DTT ECRH system design, Fusion Eng. Des. 168 (Jul. 2021) 112678, https://doi.org/10.1016/J.FUSENGDES.2021.112678. Art. no.
[3] F. Fanale, et al., Status of DTT ECH Transmission lines and Antennae, IEEE Transac. Plasma Sci. (Apr. 2024), https://doi.org/10.1109/TPS.2024.3382745.
[4] A. Moro, et al., Progress and challenges of the ECH transmission line design for DTT, Fusion Eng. Des. 202 (May. 2024), https://doi.org/10.1016/J.FUSENGDES.2024.114391.
[5] D. Busi, et al., In-vessel piezoelectric actuation system for DTT ECRH launchers: conceptual design, Fusion Eng. Des. 180 (Jul. 2022) 113196, https://doi.org/10.1016/J.FUSENGDES.2022.113196.
[6] E. Gajetti, et al., A new efficient mirror cooling for the transmission line of fusion reactor ECH systems based on triply periodic minimal surfaces, IEEE Transac. Plasma Sci. (Apr. 2024), https://doi.org/10.1109/TPS.2024.3383275.
[7] X. Wang, et al., Research activities and progress on the long pulse ECRH launcher for EAST, in: Proc. EPJ Web Conf, 2019 02012, https://doi.org/10.1051/epjconf/201920302012.
[8] M. Joung, et al., Design of ECH launcher for KSTAR advanced Tokamak operation, Fusion Eng. Des. 151 (Feb. 2020) 111395, https://doi.org/10.1016/J.FUSENGDES.2019.111395. Art. no.
[9] V. Erckmann, et al., Electron cyclotron heating for W7-X: physics and technology, Fusion Sci. Technol. 52 (Aug. 2007), https://doi.org/10.13182/FST07-A1508.
[10] H. Hailer, et al., Mirror development for the 140 GHz ECRH system of the stellarator W7-X, Fusion Eng. Des. 66-68 (Sep. 2003) 639–644, https://doi.org/10.1016/S0920-3796(03)00264-3, vols.
[11] A.Mas Sanchez, et al., Fluid-dynamic and thermo-mechanical analyses of the ITER electron cyclotron Miter bend mirror for the off-centered beam scenario, Fusion Eng. Des. 192 (Jul. 2023) 113643, https://doi.org/10.1016/J.FUSENGDES.2023.113643. Art. no.
[12] F. Sanchez, et al., Design and manufacturing of the ITER ECRH upper launcher mirrors, Fusion Eng. Des. 84 (Jun. 2009) 1702–1707, https://doi.org/10.1016/J.FUSENGDES.2009.01.013.
[13] P.Santos Silva, et al., Design concept and thermal-structural analysis of a high power reflective mm-wave optical mirror (M2) for the ITER ECH-UL, Fusion Eng. Des. 146 (Sep. 2019) 618–621, https://doi.org/10.1016/J.FUSENGDES.2019.01.037.
[14] D. Busi, et al., Study of magnetic effects on DTT ECRH front-steering mirror, Fusion Eng. Des. 191 (Jun. 2023) 113550, https://doi.org/10.1016/J.FUSENGDES.2023.113550. Art. no.
[15] A. Allio, et al., Assessment of the performance of different cooling configurations for the launcher mirrors of the ECRH system of the DTT facility, IEEE Transac. Plasma Sci. 50 (11) (Nov. 2022).
[16] E. Gajetti, et al., Development of a novel TPMS cooling structure for the launcher mirror M2 of the DTT ECH system, Present. 33rd Sympos. Fusion Technol. (Sep. 2024).
[17] A. Salvitti, et al., Preliminary design and thermal analyses of the steerable mirror cooling channel of the DTT ECRH, Fusion Eng. Des. 161 (Dec. 2020) 111880, https://doi.org/10.1016/J.FUSENGDES.2020.111880. Art. no.
[18] P. Goldsmith, Quasioptical Systems, IEEE Press, 1998.
[19] B. Bird, “Transport phenomena”, 2001.
[20] Siemens CD-Adapco, STAR-CCM+ User Guide (2020).
[21] A. Allio, et al., Assessment of the performance of different cooling configurations for the launcher mirrors of the ECRH system of the DTT facility, Presented 29th IEEE Sympos. Fusion Eng., Virtual (Jul. 2021).